Acta Mechanica Sinica (2021) 37(7):1090–1103
https://doi.org/10.1007/s10409-021-01099-7

RESEARCH PAPER

Effect of surface roughness on the aerodynamics of a high-speed train subjected to crosswinds

M. Y. Wang[1,2] · S. A. Hashmi[3] · Z. X. Sun[1,2] · D. L. Guo[1,2] · G. Vita[3] · G. W. Yang[1,2] · H. Hemida[3]

Received: 1 March 2021 / Accepted: 19 March 2021 / Published online: 2 July 2021
© The Chinese Society of Theoretical and Applied Mechanics and Springer-Verlag GmbH Germany, part of Springer Nature 2021

Abstract
The irregularities on trains bodies are normally ignored or greatly simplified in studies concerned with aerodynamics. However, surface roughness is known to affect the flow characteristics in the boundary layer near the wall, hence potentially influencing the aerodynamic performance of a train. This work investigates the effects of roughness on the overall aerodynamic characteristics of a high-speed train subjected to crosswinds. Both experimental work and numerical work have been conducted to simulate a typical high-speed train with a 90° yaw angle, with both a smooth and rough surface. Roughness is applied to the roof of the train surface in the form of longitudinal strips. Results reveal that the addition of roughness is able to reduce the surface pressure on the roof and leeside of the train. Numerical results agree well with experimental ones and confirm that an increase in the roughness relative size can effectively restrain flow separation and reduce surface pressure. Moreover, numerical simulation results show that side force coefficient and roll moment coefficient subjected to rough model significantly decreased compared with smooth model. The conclusions drawn in this study offer the chance to derive critical reference values for the optimization of the aerodynamic characteristics of high-speed trains.

Keywords High-speed train · Surface roughness · Crosswinds · Aerodynamics · Flow separation

1 Introduction

High-speed trains are known to play an important role in public transportation around the world and are supported in several places, such as the European Union, China, Korea, and France [1]. There have been clear indications that in the upcoming years it is likely that rail passenger numbers are going to double [2]. As a result, it is important to develop high-speed and highly efficient trains. Also, since train bodies serve for a long period of time, their geometric features must be chosen carefully. As Diedrichs discussed in Ref. [3], designing high-speed trains to be lighter and longer is the current aim in the optimization of railway vehicles. This is done mainly to ensure savings in travel times. However, this results in potential risks for the train bodies. A train body subjected to crosswinds is surrounded by a complex flow field. This may lead to steady and unsteady aerodynamic forces acting on the vehicle. Derailment or even overturning of trains is plausible under the action of strong crosswinds [4]. To improve the safety of trains, a number of measures have been realized. These include design improvements made with the aim of improving the external aerodynamics of the train bodies. Such design improvements include ensuring low center of gravity for the trains, avoiding protruding objects on the roofs, large roof radii corners, sufficiently low external roof heights, favorable cross-sections, and streamlined front ends [3]. In fact, Browand et al. [5] mentioned in their study that design factors may have a strong influence on the stability of train bodies. Therefore, assessment of crosswind stability of high-speed trains with different design features is an important subject. References [6–8] suggest some important requirements and test procedures for crosswind assessments of railway vehicles. EN 14067-1 and BS EN 14067-6 are amongst the several standards which present details about methods for assessing train stability in

Executive Editor: Yue Yang.

✉ Z. X. Sun
sunzhenxu@imech.ac.cn

[1] Key Laboratory for Mechanics in Fluid Solid Coupling Systems, Institute of Mechanics, Chinese Academy of Sciences, Beijing 100190, China

[2] School of Engineering Science, University of Chinese Academy of Sciences, Beijing 100190, China

[3] School of Civil Engineering, University of Birmingham, Birmingham B15 2TT, UK

crosswinds through various tests such as full-scale, model-scale and numerical. Also, one of the important parameters for assessment of trains in crosswinds is the angle of wind attack.

A number of experimental as well as numerical studies have investigated the aerodynamic response of trains under the impact of crosswinds [4,9–11]. To elaborate, these works considered the various factors which can have an influence on the stability of a train in strong crosswinds with varying yaw angles. For instance, Hemida and Krajnović [12] performed a numerical study to explore the influence of the shape of a train nose on the flow structures, which develop around trains, under varying yaw angles. In their study, numerical simulations were performed on train models with either a long nose or a short nose. The results from their study showed that the short nose model resulted in highly unsteady and three-dimensional flows around the nose. These flows were found to yield more vortices in the wake as compared to the long nose train model. Therefore, the study concluded that comparatively, the short nose not only influenced the surface flow but also had an impact on the dominating frequencies. These resulted from the flow instabilities in the shear layer. Another study by Cheli et al. [13] investigated the influence of infrastructure scenarios on the aerodynamic loads acting on a train body. In their study, they made use of the ETR500 train and considered different infrastructure scenarios: embankment, viaduct and flat ground with and without ballast and rail. The study was able to highlight the influence of the different infrastructure scenarios on the aerodynamic loads. Furthermore, Hashmi et al. [4] studied the aerodynamic performance of a passenger train with and without different shapes of windbreak walls, under varying yaw angles, inside a wind tunnel. The results from the study showed clear differences in terms of pressure distribution around the train surface with the use of all types of windbreak walls in the windward side, as compared to cases without any use of a windbreak wall.

While these recent works provided noteworthy insights on train aerodynamic properties for different test cases, most of these studies did not consider the effects of roughness on train surfaces. Roughness in this context refers to an irregularity, which may occur on the surface of the train due to a geometric feature. Usually, the works performed in the past have considered smooth train surfaces by often ignoring some details in the geometry of train bodies. This is usually done in experimental tests to ease the process of constructing a scaled model. Whereas, in numerical works, it might be practically difficult to reproduce an exact replication of the full-scale model and often some unnecessary details may be simplified to create ease in meshing the geometry and performing numerical simulations. However, in reality, most trains have external protruding objects fitted to their bodies. These may include exterior cameras or train indicator lights. While these can be expected to have a minor or even negligible influence on the flows around trains and the safety of the trains, these may be ignored. However, certain objects fitted on the train exteriors may have an influence on the flow around the train. For instance, certain trains have pleated structures on the roof to reinforce strength to the train body while some trains have rain cover eaves to prevent water deposition. These geometric features can be expected to influence the flow fields around trains and can have a considerable effect on the stability of the formed boundary layers on train surfaces. In fact, it can be anticipated that such external structures can result in various flow separations and reattachments and thus lead to changes in the aerodynamic forces experienced by train surfaces.

Although there are few studies on the influence of train surface roughness on aerodynamic characteristics, some scholars still use different methods to study the surface roughness of the train running in the open air. Wang et al. [14] designed a diamond texture on the surface of a carriage to achieve roughness. After solving and analyzing the noise distribution, it was concluded that optimizing the diagonal ratio and depth-to-side ratio of the texture can effectively reduce the air frictional noise of running train. Miao and Gao [15] numerically investigated the influence of ribs on the aerodynamic performance of a train. The results from their study revealed that the use of convex ribs was able to change the resulting lift force coefficient of the train from negative to positive, when compared to the case with no ribs. Zhang et al. [16] compared the aerodynamic resistance before and after adding pits in the bogie area of the intermediate car of a train, and the results showed that the non-smooth surface can reduce the drag of the intermediate car. Zhu et al. [17] mounted ball sockets to the surface of the car body of a high-speed train, in order to control the turbulence characteristics of the boundary layer. The simulation results showed that adding ball sockets only to the tail car is beneficial for the reduction in train drag. García et al. [18] used Large Eddy Simulation (LES) method to study the aerodynamic behavior of a full scale train under synthetic crosswind for both smooth and rough train surfaces. An important conclusion can be drawn, compared to the smooth surface, the rough surface makes the average value of the yaw moment coefficient of the train decrease, while the average value and extreme value of other aerodynamic coefficients increase. Liu et al. [19] studied the aerodynamics of the rods based on bionic non-smooth structures for the reduction of noise and drag of the pantograph. They found that corrugated groove rob is the best bionic design, which can effectively reduce drag and noise. Tang et al. [20] established 24 V-groove models by changing the apex angle and height. According to the numerical calculation results, the V-shaped groove with a height of 100 μm and an apex angle of 40° has the highest drag reduction rate of 10.09%.

As detailed above, not much data is presented in the literature, which examines the aerodynamic response of trains with irregular surfaces, specifically in an experimental manner. As Dorigatti et al. [9] discussed that numerical simulations do play a key role in the evaluation of train performances but are not yet considered sufficient in terms of accuracy for designing purposes [6–8]. The wind tunnel experiment can directly show whether there is an influence of roughness on the surface pressure of the train, and at the same time ensure the accuracy of the data. However, accurate numerical simulation can intuitively show the influence of roughness on the flow field around the train, and also it can directly give the difference in the aerodynamic force of the train under different roughness conditions. Therefore, it is important that the concept of irregular train surfaces is investigated both experimentally and numerically in order to better understand how such surfaces can affect the flow around a train subjected to crosswinds.

This paper presents the analysis of the results obtained from both experimental and numerical ways, to better understand the mechanism of surface roughness on a high-speed train subjected to crosswind conditions. Concisely, the research is aimed at providing an understanding of flow mechanism and aerodynamic characteristics on a 1:25 scaled passenger train model subjected to crosswinds, both with and without irregular roof surfaces. Section 2 introduces the experimental and numerical methodology adopted in this research. Section 2.1 describes the wind tunnel facility, scaled models and experimental setup, while Sect. 2.2 includes the numerical algorithm, computational models, computational domain, boundary conditions and computational mesh. Section 3 compares experimental results and numerical results of surface pressure coefficients on different sections for the smooth and rough models, which confirms the validation of the results. Section 4 provides the results of the experimental work with a discussion of the findings. Analysis and discussion on these results are presented in addition to providing the numerical results to understand the influence of local roughness on the surface pressure distribution and the surrounding flow structures of the high-speed train. Finally, Sect. 5 concludes the research by listing the main research outcomes along with providing suggestions for future work.

2 Methodology description

2.1 Experimental setup

2.1.1 Wind tunnel facility

The experimental work in this research is performed at the University of Birminghams (UoB) wind tunnel facility. The wind tunnel has a cross-sectional area of 2 m by 2 m and has a 10 m long working test section. 49 axial fans are used to provide the required wind flow at the inlet of the wind tunnel through a honeycomb screen, which allows the provision of a uniform wind speed with minimum turbulence. For measuring the three-dimensional flow velocities, series 100 cobra probes with 2 kHz [21] are used. Prior to any experimental work, characteristics of the flow inside the wind tunnel are determined.

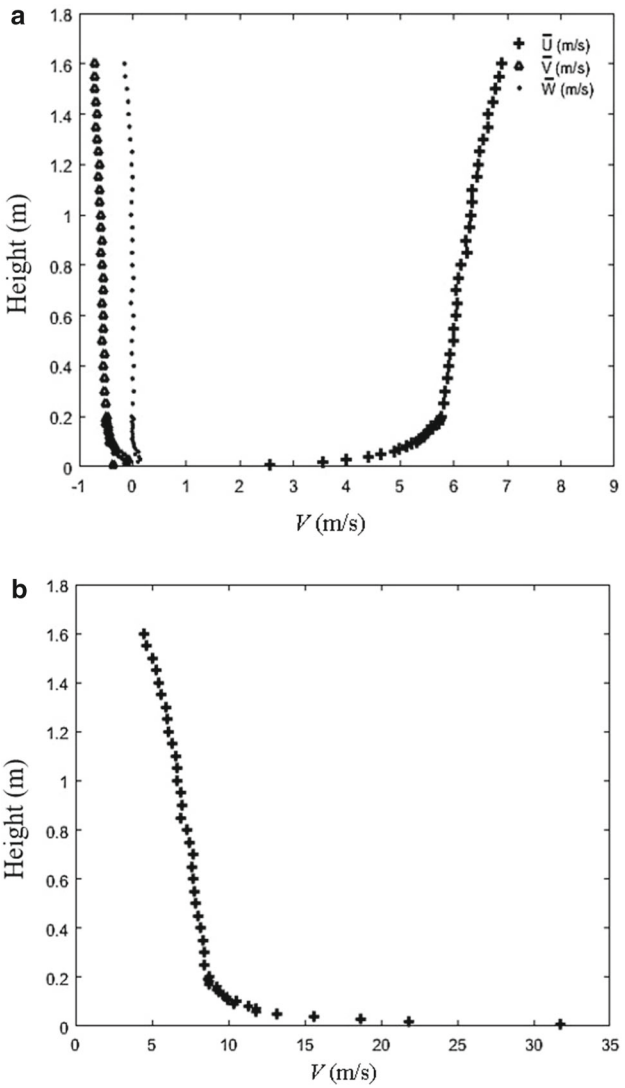

Fig. 1 Characteristics of the flow inside the wind tunnel. **a** Vertical wind profile (VWP) for the streamwise ($\overline{U}$), lateral ($\overline{V}$) and vertical ($\overline{W}$) mean velocities. **b** Streamwise turbulence intensity (%) at the center of the wind tunnel

Figure 1a shows the vertical wind profile (VWP) for the streamwise mean velocities ($\overline{U}$), lateral mean velocities ($\overline{V}$) and vertical mean velocities ($\overline{W}$), respectively, in the wind tunnel while Fig. 1b illustrates the streamwise turbulence intensity inside the wind tunnel. It must be noted that these profiles are measured without any models at the exact place where the train model is located in the experimental runs. As

discussed in Ref. [4], the presence of a splitter plate does not modify the wind speed profile, especially in the section where the train model is placed. Based on the horizontal wind profile measurements, the spanwise average of the streamwise mean velocities ($\overline{U}$) is considered as 7.2 m/s. The average streamwise turbulence intensity is 5.5%, as shown in Fig. 1b.

2.1.2 Scaled models and experimental setup

As noted in Sect. 1 of this paper, this work is aimed at investigating the effect of surface roughness on the aerodynamic flow around a train body. To do so, experiments are firstly performed on a smooth train surface and a rough train surface, for comparison purposes. A 1:25 scaled model of the Class 390 Pendolino train is used, which includes a leading car and a half-trailing car. Table 1 gives the similarity parameters of scaled model and prototype. The experiments are performed at a yaw angle of 90°. To represent surface roughness, longitudinal strips of PVC material are used in a pleated manner on the roof of the train. Experimental investigation is only carried out on the leading car. The existence of the half-trailing car reduces the influence of wake flow close to the leading car and ensures a realistic flow around it [8]. In terms of the ground scenario, a single track and ballast rail (STBR) is adopted. For experiments, the testing section is positioned at 6 m from the inlet of the wind tunnel, as shown in Fig. 2. And the splitter plate is located at a height of 0.3 m from the wind tunnel floor, which can eliminate the impact of ground effects.

Table 1 Similarity parameters of scaled model and prototype

	Scaled model	Prototype
Length of the leading car (m)	1	25
Length of the half-trailing car (m)	0.5	12.5
Height of the train (m)	0.156	3.9
Width of the train (m)	0.11	2.75

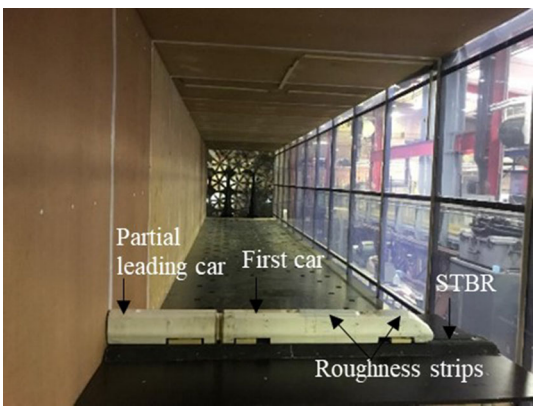

Fig. 2 Experimental set-up of the train model at a yaw angle of 90° inside the wind tunnel

The leading car is equipped with a 162 pressure taps, and assembles in a series of 14 loops (A-N) in a longitudinal direction of the train, as shown in Fig. 3a. The pressure taps are connected to a 500 Hz multi-channel pressure-system (Solution for Research Ltd) with the use of PVC tube connections. The pressure measurement system allows for measuring the surface pressures on scaled models. The mean pressure for a single pressure tap is obtained by time averaging the instantaneous data that have been collected, for a period of three minutes. Figure 3b illustrates the coordinate system used with reference to the wind. Table 2 provides the longitudinal position of each loop, where L is the first car's total length, i.e. is 1 m.

2.1.3 Description of the test cases

The following two experiments are conducted in this study:

(a) train with smooth surface at a yaw angle of 90°,
(b) train with a rough surface at a yaw angle of 90°.

For the experiments concerning rough surfaces, PVC strips with height and width of 1 mm and 2 mm, respectively, are glued on the roof of the train in a longitudinal direction of the train length in a pleated manner. As illustrated in Fig. 4a, loops D, E, G, H and I are under the influence of these roughness strips. Figure 4b shows the roof of a typical high-speed train with a rough surface.

2.2 Numerical setup

2.2.1 Numerical algorithm

Numerical simulations are one of the most diffused methods to analyze the aerodynamic characteristics of trains, where the selection and establishment of a suitable turbulence model is the key in the entire process. The turbulence models commonly used to study train aerodynamics are the large eddy simulation (LES) model [22], Reynolds-averaged Navier-Stokes (RANS) model [23] and the detached eddy simulation (DES) model.

Spalart et al. [24] proposed the DES model, which is a coupled hybrid model formed by the combination of the LES and RANS models. The advantage of RANS lies in the small amount of calculation needed which can effectively shorten the calculation times, while the main advantage of LES is that it has a very high calculation accuracy, which greatly improves the credibility of the calculated results. As a combination of the two, DES naturally has these advantages and thus can simulate complex three-dimensional unsteady turbulent flows. The improved delayed detached eddy simu-

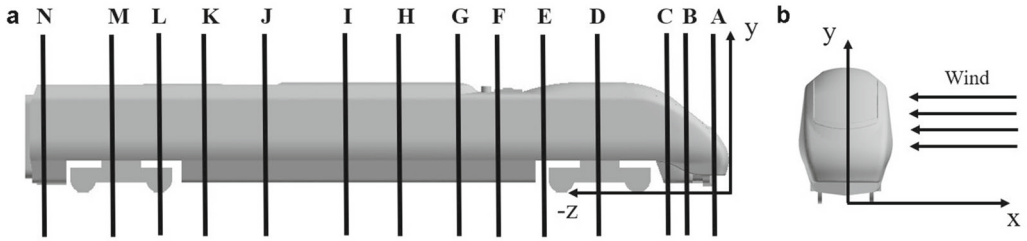

Fig. 3 **a** Position of the loops and **b** coordinate system with reference to wind

Table 2 Similarity parameters of scaled model and prototype

Loop	A	B	C	D	E	F	G	H	I	J	K	L	M	N
$-z/L$	0.018	0.055	0.085	0.185	0.25	0.325	0.39	0.48	0.56	0.665	0.75	0.81	0.89	0.97

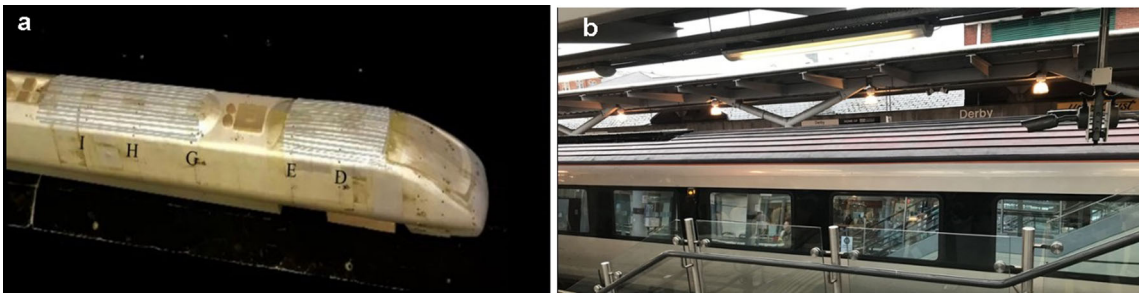

Fig. 4 **a** Demonstration of the added roughness strips and their respective positions in terms of the loops D, E, G, H and I; **b** roof of a typical high-speed train with a rough surface

lation (IDDES) model is developed as an improved version of the DES model. Combined with the wall-modeled large eddy simulation (WMLES) model [25], this IDDES model can effectively deal with those grids which are solved by RANS/LES model at the same time in the logarithmic region, and reduce the grid correlations. Li et al. [26] used IDDES model to analyze the flow fields, surface pressures and aerodynamic forces obtained around the train subjected to crosswinds, and the results show that this method can accurately predict the average flow field around the train.

In this paper, the Mach number of the incoming flow in the domain is less than 0.3, so it is assumed that the air flow is incompressible. This study uses the IDDES method based on SST k-ω two-equation model to simulate the influence of local roughness on the surface pressure distribution and the surrounding flow field structures of a high-speed train. For unsteady calculations, the time step is set as 0.001 s and the number of inner iterations is 20. Since the simulation tends to converge within 0.6 s, the total computational time is set to be 1 s.

2.2.2 Computational models

The numerical setup has been developed paying a great deal of attention to the CAD geometry. As experimental work performed at the University of Birminghams wind-tunnel facility is used to validate the numerical simulations in this work, exact dimensions of the train model, the STBR and the splitter plates used in the experiments are utilized for the CAD model. This is done to ensure a quality validation of the numerical simulations. The geometry of the train CAD model with dimensions is shown in Fig. 5.

Similar to the experimental work, a series of longitudinal strips are added on the roof of the leading car to obtain a

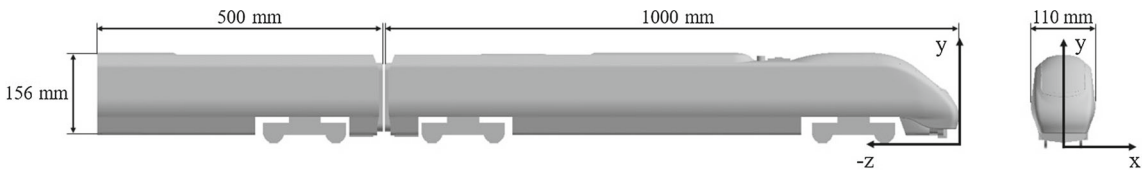

Fig. 5 Computational model of the smooth train

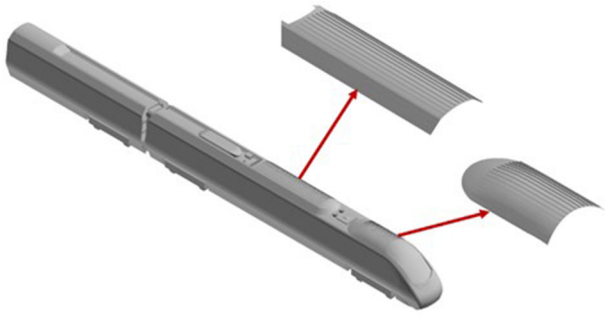

Fig. 6 Computational model of the rough train

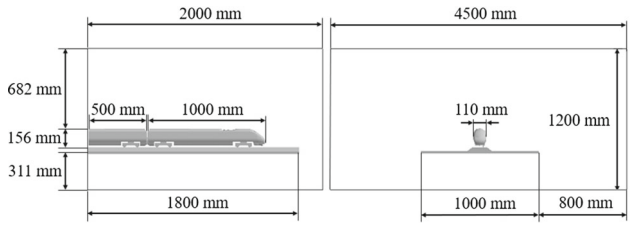

Fig. 7 Computational domain used in the numerical simulation

model with a rough surface, as illustrated in Fig. 6. There are 15 strips on each of the two enlarged areas. The cross-sectional areas of all the strips are identical, where each strip is 2 mm wide and 1 mm high. However, the lengths of strips on the frontal region are 0.12 m, while the lengths of strips on the latter region are 0.24 m, based on the geometric designs of the two areas.

2.2.3 Computational domain and boundary conditions

Figure 7 shows the position of the train model in the computational domain, including a STBR and a splitter plate. To ensure precise validation, the dimensions and details of the numerical models are kept consistent with the experimental models.

In terms of the boundary conditions, all boundaries are set as non-slip walls, except for the inlet and outlet boundaries. A uniform velocity is assigned to the inlet boundary while the outlet is set as a zero-pressure outlet, as demonstrated in Fig. 8. The train model along with the STBR and the splitter plate are stationary and subjected to a relative wind with a yaw angle of 90°. The crosswind speed is 7.2 m/s, and the direction is negative along the x-axis. As mentioned earlier, all these aspects are in line with the experimental campaign.

2.2.4 Computational mesh

The volume mesh generated is a trimmer mesh, mainly consisting of hexahedrons, and the prism layer grid generation on the train wall can better reflect the flow field distribution around the car body. In order to achieve the natural transition

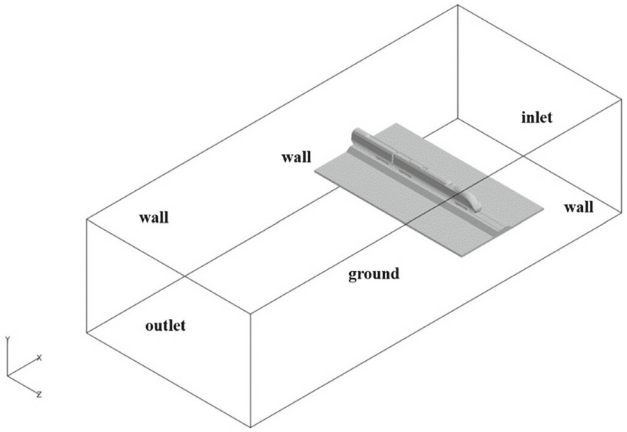

Fig. 8 Boundary conditions used in the numerical simulation

with the hexahedral mesh and to ensure a high mesh quality, a total of 10 prism layers are set up at the train surface. The total thickness of the prism layer is 0.0002 m, and the growth ratio is set at 1.1. This sizing gives an average of nondimensional wall distance, y^+, of approximately 1.13.

Due to the limitation of computational resources, the number of cells in the model has been optimized with four different densified areas set up to divide the computational domain into refinement regions. The basic size of the grid is 0.04 m, and the grid sizes of the four refinement areas from large to small are 0.0192 m, 0.0048 m, 0.0024 m and 0.0006 m respectively. For the analysis of two train models (i.e. with roughness and without roughness), the location and size of the refinement areas are same, as shown in Fig. 9. Figure 10 shows the grid distribution at position of the strips, where the generated prism layers are locally magnified for visual inspection.

3 Result validation

For both the experimental tests, loops A to N are investigated where loop A is located at the nose of the train and loop N is situated at the tail of the train. Each loop represents a cross-section of the train and can be split into four sections: the windward side (WWS), the roof (ROOF), the leeward side (LWS) and the underbody (UB). This section represents the results of surface pressure in a polar coordinate form, as shown in Fig. 11.

The main aim of this research is to investigate the effect of a rough train surface on the flow which forms around a train body. However, prior to that, it is important to first obtain data for a train model with a smooth surface. Such a case will act as a benchmark and assist in demonstrating the intensity of the change in the results obtained. As mentioned in Sect. 2, roughness is introduced on the roof of the train in the form of longitudinal strips, arranged in a pleater manner. The pressure

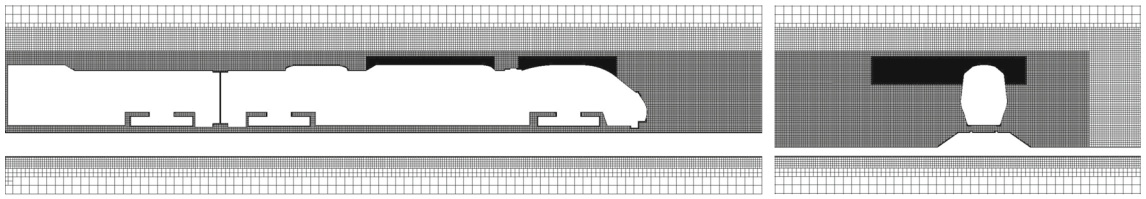

Fig. 9 Distribution of grids on the different sections

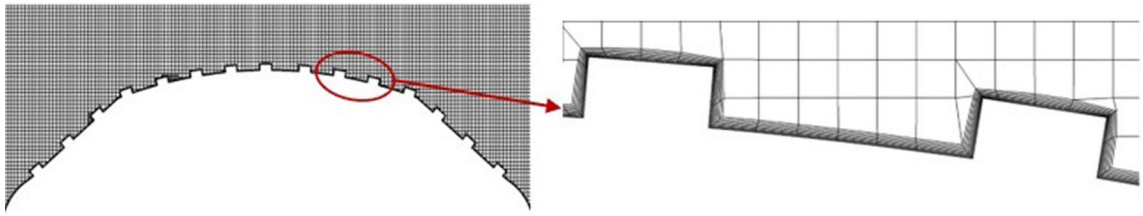

Fig. 10 Grid distribution around the strips

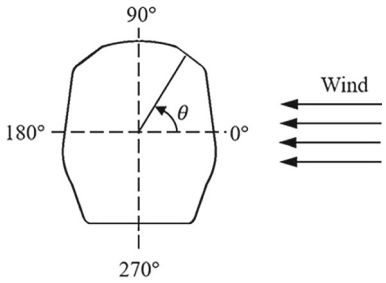

Fig. 11 Orientation of angle θ with respect to wind [4]

distribution results obtained over the train surface for the experiments and simulation at a yaw angle of 90° can be expressed in terms of a non-dimensional pressure coefficient C_p, and it is defined as follow:

$$C_p = \frac{P - P_0}{0.5\rho V_{\text{ref}}^2}, \tag{1}$$

where $P - P_0$ represents the difference between the local static pressure and the free-stream pressure, ρ is the airflow density, which takes the value of 1.185 kg/m^3, and V_{ref} is the wind velocity, which is 7.2 m/s.

To validate the experimental and numerical results, two typical loops E and G are selected. These two loops are located in the area of increased roughness, which is convenient for visual observation of the influence of local roughness on the surface pressure distribution. Figure 12 shows the comparison between the experimental results and the numerical calculation results of the pressure coefficient C_p on the loops E and G. The experimental and numerical results of Fig. 12a and c correspond to the smooth model, while all the results of Figs. 12b and d are obtained using the rough model. It is not difficult to see that the CFD results are in good agreement with the test results, which proves that the calculation results obtained using the IDDES method are accurate.

As shown in Fig. 12a, the first and the last test points are located near the stagnation point, so the pressure coefficient values are both large. When the airflow moves to the second test point, the flow rate gradually increases, and the pressure coefficient value decreases. It is easy to know from the numerical result that flow separation occurs between the second and third test points, and the pressure coefficient appears to be a minimum. At the same time, it can be seen from Fig. 12b that the existence of rectangular strips can increase the minimum value of the pressure coefficient and weaken the suction generated by the acceleration of the flow. From the middle position of ROOF to the middle position of LWS, differences among the pressure coefficients of test points are small, and the numerical result curve doesnt have obvious fluctuation, which indicates that flow reattachment may occur after flow separation. When the airflows from ROOF and UB merge at the LWS, it will cause larger disturbance, which leads to the second flow separation and another minimum pressure coefficient. In addition, the radius of curvature of the UB is basically same, so the pressure coefficient is in a stable state.

It can be seen from Fig. 12c that the first and the last test points on loop G of smooth model also have large pressure coefficient values. And with the continuous movement of the airflow, the pressure coefficient value gradually decreases. What is different from loop E is that the airflow has already begun to separate before reaching the second test point. When it reaches the third test point, flow reattachment occurs, but then flow separation occurs again and ends at the middle position of ROOF. The reason for this phenomenon is most likely that different geometric shapes lead to each point has different radius of curvature, which makes the surface pressure

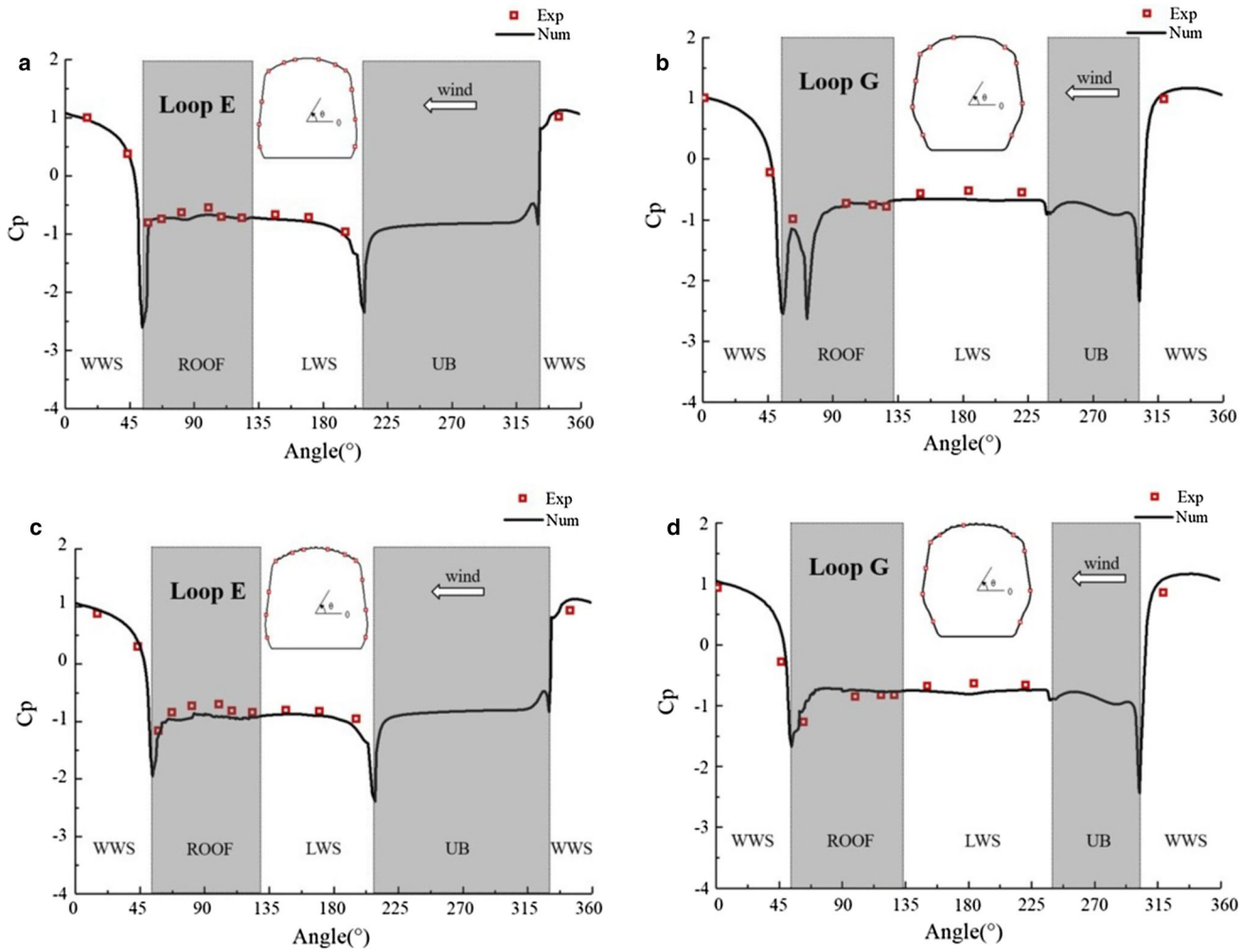

Fig. 12 Comparison of C_p along loops E and G between numerical and experimental results: **a, c** smooth model and **b,d** rough model

change significantly. From the fourth test point to the bottom of the LWS, the pressure coefficient value has remained stable. However, the pressure coefficient value of the UB area is not as stable as the same area of E loop, and has a gradually decreasing trend. This difference may be due to the UB of G loop is closer to the track than the UB of E loop, so it is more affected by the track. According to Fig. 12c and d, it can be verified again that the rectangular strips help to inhibit flow separation, reduce the strong suction on the train surface, and improve local aerodynamic performance in a way.

4 Results and discussions

4.1 Comparison of surface pressure coefficients

In order to better comprehend the influence of a rough roof surface on the flow which exists around a train body, the relative difference for each pressure tap can be calculated. Hence, in this study, the relative difference (RD) is defined by

$$RD = \frac{\overline{C}_{\text{P-Rough}} - \overline{C}_{\text{P-smooth}}}{\overline{C}_{\text{P-smooth}}} \times 100\%, \tag{2}$$

where $\overline{C}_{\text{P-Rough}}$ and $\overline{C}_{\text{P-smooth}}$ are the mean non-dimensional pressure coefficients for each tap with a rough roof surface and smooth roof surface, respectively.

Figure 13 illustrates the mean surface pressure coefficient distribution at loops D, E, G and H for the smooth and rough train surface at a yaw angle of 90°. In terms of the results obtained with both the surfaces, it is apparent that the trend followed by the C_p distribution around the train body is quite similar for both the cases. However, as expected there are slight differences in the magnitude of C_p obtained. Generally, for all loops (A-N), the WWS demonstrates positive results with negative values obtained for regions with flow accelerations. Furthermore, as the flow transits from the WWS to

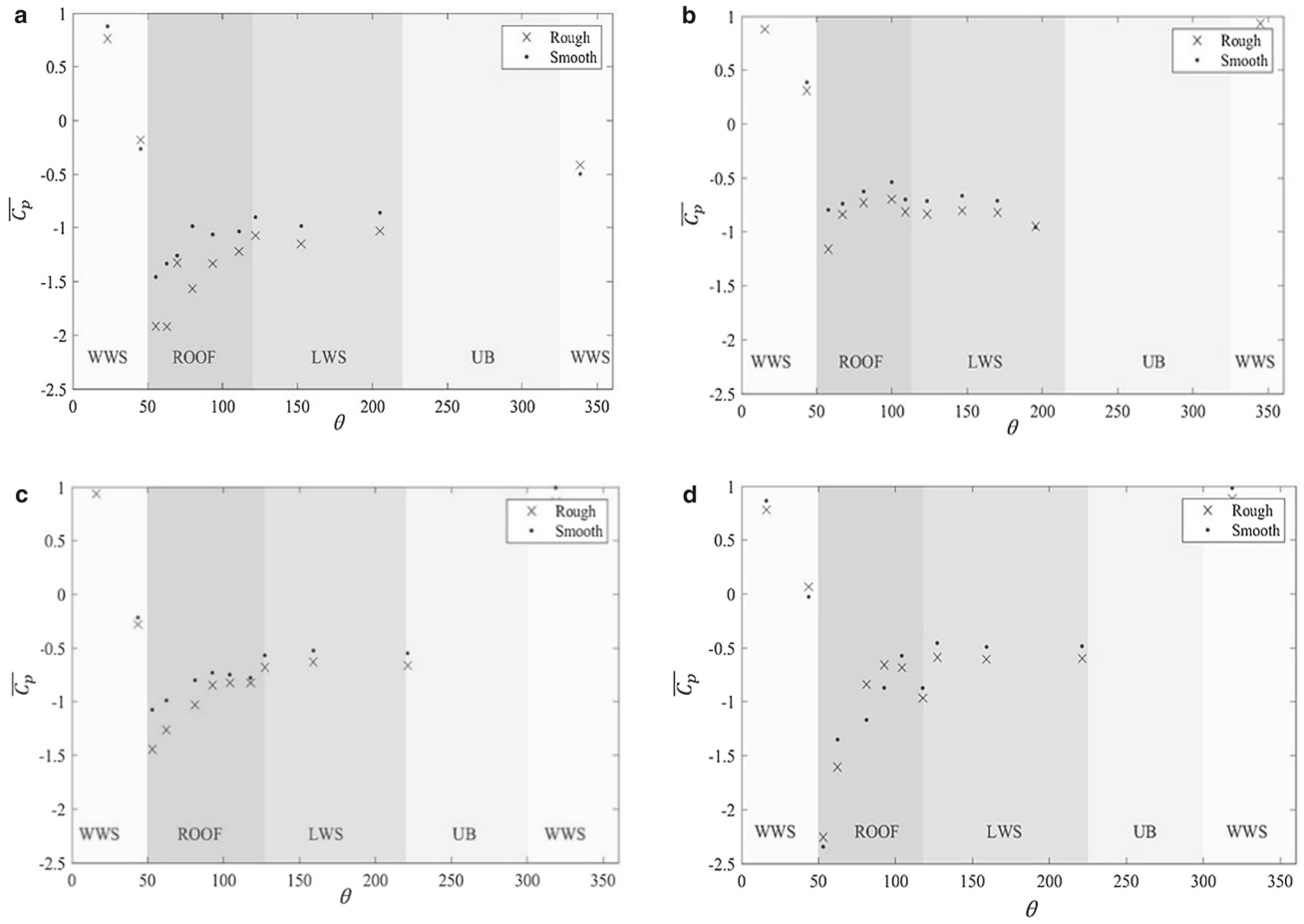

Fig. 13 Comparison of the mean surface pressure coefficient distribution at different loops for the rough and smooth train surfaces at a yaw angle of 90°: **a** loop D; **b** loop E; **c** loop G; **d** loop H

the ROOF, the C_p values tend to decrease, indicating flow accelerations.

Figure 13a illustrates the mean surface pressure distribution on loop D for the two cases examined. In terms of the WWS, this is the surface where the flow is expected to impinge directly. The surface pressure coefficients in this region tend to be quite similar, comparatively as can be seen in Fig. 13a. This can mainly be due to no roughness present on the WWS. However, as the flow progresses towards the roof, there are apparent differences in the results obtained in the C_p obtained for the two cases. While a decrease in the C_p values is noticeable for both the cases as the flow transits from the WWS to the ROOF, the effect of roughness is evident. The introduction of roughness on the roof of the train results in much lower C_p values, indicating strong suctions, as compared to the C_p results obtained with a smooth roof surface. To elaborate, at $\theta = 55.3°$, the flow is in a transition region from the WWS to the ROOF. The windward edge of the roof has a major influence on the flow, indicating flow acceleration. For the smooth surface of the train, the C_p results demonstrate a strong suction peak. However, with the rough roof surface, a stronger suction is evident, comparatively. In terms of the flow that exists on the roof, it is apparent that the rough surface results in an overall lower C_p distribution (i.e. larger negative values are obtained) as compared to the results achieved with a smooth roof surface. One interesting finding lies at $\theta = 70°$, where the addition of roughness seems to not have an influence in the results obtained for both cases. Another interesting finding is that while for the smooth surface it can be observed that the flow stabilizes from somewhat the middle of the roof all the way to the LWS, this is not exactly the case for the flow which develops with the rough surface. To elaborate, for the rough surface, from the middle of the roof, the C_p results tend to increase thus showing pressure gradients before the flow stabilises in the LWS. For loop D, a relative difference between the two cases examined is quite visible with a maximum value of 59% for the pressure tap located at $\theta = 80°$, which corresponds to a pressure tap located close to the middle of the roof. Such a RD clearly indicates the influence of the roughness strips on the pressure distribution around the train body. In addition, from the results, a smooth roof surface

presents a laminar boundary layer. However, with the addition of roughness strips, the surface encounters a turbulent boundary layer.

Quite similarly, for loops E and G, as shown in Fig. 13b and c, the C_p distribution for the rough roof surface presented overall lower values as compared to the values obtained with the smooth roof surface. However, the trend adopted by the C_p distribution over the roof of the train is slightly different as compared to loop D. To elaborate, while a noticeable relative difference is apparent between the results of the smooth and rough roof surfaces, the maximum RD for loop E was observed at $\theta = 58°$ with a value of 45.8%. The position of the corresponding pressure tap was close to the windward edge of the roof. This was also the case in loop G. One reason behind this finding can be due to the overall geometry of the train where the roof of the train has different geometric curvatures at different cross-sections. Also, as demonstrated in Fig. 4, loop D was somewhere in the middle of the area covered by the strips. Whereas, loop E was located towards the end of the longitudinal strips and loop G was located at the beginning of the second set of longitudinal strips.

In terms of loop H, a slightly different trend is observed in the achieved C_p distribution compared to other loops for the two cases examined. The results obtained on loop H in terms of C_p distribution are illustrated in Fig. 13d. The strong suction peak observes at $\theta = 58°$ remained. However, on this loop, the airflow seems to be agitated in a much more complex manner as compared to other loops. Also, as seen in other loops where the rough-roof surface usually results in overall lower C_p distribution, it is not the case for this loop. For this loop, mainly on the roof, lower C_p values with a smooth roof surface can be observed at certain pressure taps. An increase along with fluctuations in surface pressures with the rough surfaces is evident.

4.2 Characteristics of the flow field

Figure 14 shows the pressure coefficient contour of the train surface for the smooth and rough models. As shown in Fig. 14a and b, when the wind impinges directly on the train surface, stagnation regions will appear on the WWS of the train, resulting in extremely high surface pressure. As the flow transits from the WWS to the ROOF, the positive pressure values can be seen to decrease significantly. This is mainly due to a large suction taking place because of the flow acceleration on the windward edges of the roof. Over the roof of the model, the flow tends to demonstrate weaker suctions due to flow separations. Moreover, based on the area in the red framed box in Fig. 14a and b, it can be seen that the rough model greatly reduces the absolute value of pressure in the roof area near the windward side, indicating that the added roughness strips can reduce the flow separation on the roof. The flow

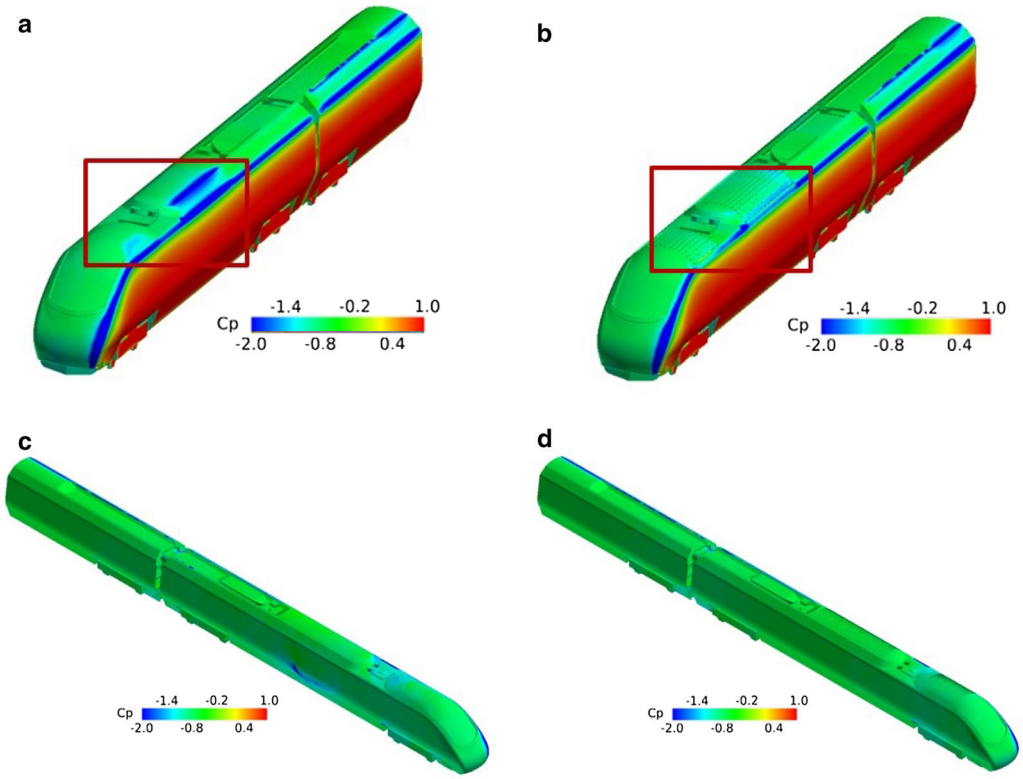

Fig. 14 Pressure coefficient contour for smooth and rough models: **a,c** smooth model; **b,d** rough model

under rough condition can tend to pass by the train surface with weak flow separations. As a result, the inviscid force of the train in the incoming flow direction can be reduced to a certain extent. The flow field becomes more favourable with the introduction of roughness. Figure 14c and d show the pressure coefficient distribution on the LWS under the smooth and rough models. It is obvious that the pressure coefficients on the LWS are all negative. However, there are still some areas with extremely low pressure on the LWS of the smooth model, while uniform C_p can be observed on the LWS of the rough model. This shows that the rough model improves the aerodynamic performance on the LWS of the train. In addition, one interesting finding details that the flow usually starts to stabilize from the middle of the ROOF to the LWS, indicating the possible flow reattachment following flow separations.

In order to observe the flow separation phenomenon on the train surface more intuitively, Fig. 15 shows the separation lines on the WWS the leading car under the smooth and rough models. It can be seen from Fig. 15 that there is basically no separation line on the WWS of the leading car, indicating that most of the airflow can flow along the wall. When the airflow moves to the junction of the WWS and the ROOF, separation line S1 is formed, which means that the flow separates here. And the separation continues until the airflow reaches separation line S2. The area between the two separation lines mentioned above is the area where significant flow separation occurs. It can be seen from Fig. 15b that under the influence of the rectangular strips, separation line S2 in Fig. 15a disappears. In addition, comparing Fig. 15a and b, it can be seen that there are almost no extra separation lines in the area where flow separation occurs on the top of the smooth model, while many short separation lines appear in the same area of the rough model, indicating that the strips destroy the flow mode of the air close to the wall, and have an inhibitory effect on large flow separation.

The iso-surface of Q-criterion, which is defined as the second invariant of the velocity tensor, can be used to identify the vortex structures around the train body. Figure 16 shows the iso-surface of Q-criterion at 50,000 for the ROOF of smooth and rough models. It can be seen that the vortex structures above the ROOF are obviously different for these two models. As shown in Fig. 16a, large-scale vortices emerge at the downstream of ROOF, which often contain higher energy. However, for the rough model, no obvious vortex structures can be found until the end of ROOF, which can be seen as that the turbulent transition has been delayed due to the roughness. The lateral force of the train can be divided into two parts: one due to the impingement of the incoming flow, and the other from the suction effect of the vortex structures near the train body. On the one hand, the existence of roughness with proper height can work as a barrier to block away the vertex structures near the train surface. On the other hand,

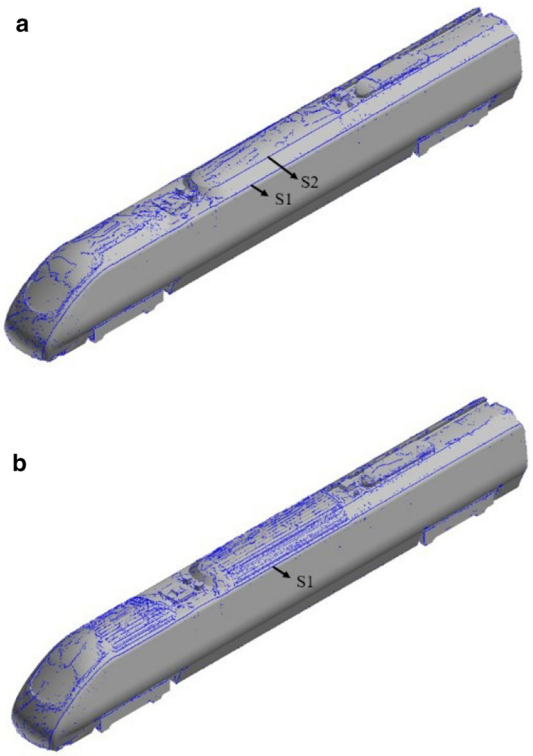

Fig. 15 Separation lines on the WWS. **a** smooth model, **b** rough model

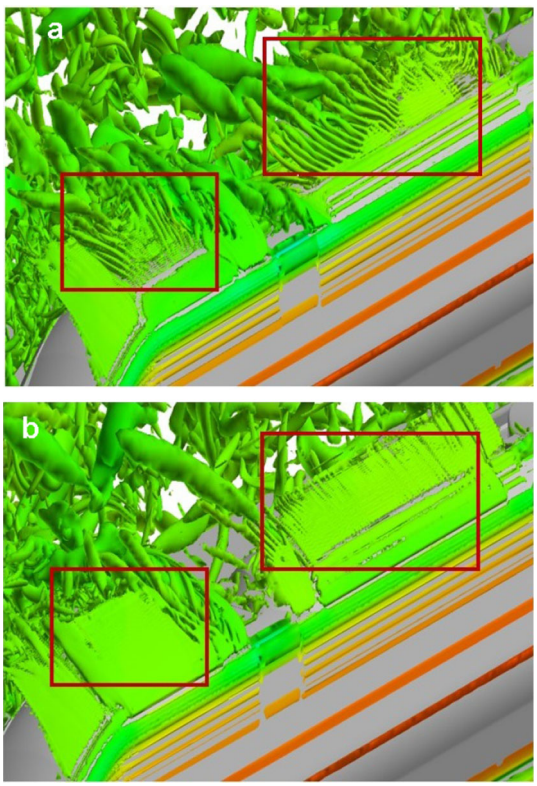

Fig. 16 Iso-surface of Q-criterion at 50,000. **a** smooth model. **b** rough model

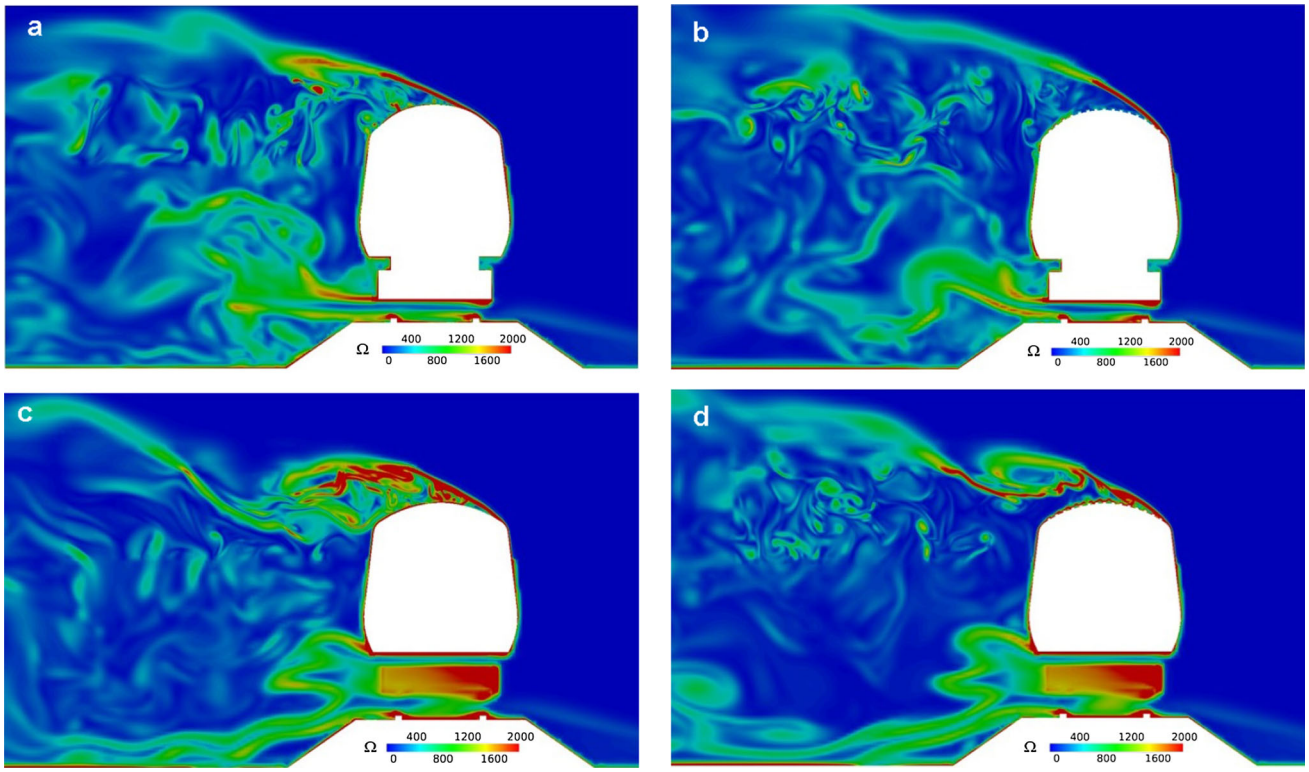

Fig. 17 Vorticity vector magnitude contour of different sections for smooth and rough models: **a** loop D of smooth model; **b** loop D of rough model; **c** loop E of smooth model; **d** loop E of rough model

the strips provide extra energy to the flow in the sublayer so that the energy exchange inside the boundary layer becomes more severe. As a result, the large-scale vortex structures have been dissipated. The intensity of the vortex structure for the rough model tends to be weaker than the that of the smooth model, so that the corresponding suction effect has been decreased, which can help reduce the lateral force and overturning moment.

Figure 17 shows the vorticity contour on the cross section at loops D and E for the smooth and rough train models. It can be seen that whether train surface is smooth or not, the airflow will form a strong vortex at the corner of the WWS and move to the LWS along the direction about 135°. In addition, due to the interference of the bogie area and the impact of ground effects, the vortex structures formed by the airflow from bottom will also have greater strength. When the airflows from the top and bottom meet, the LWS will have complex vorticity distribution characteristics.

As shown in Fig. 17a and c, there are strong vortex structures on the ROOF of loops D and E. However, in contrast, the strengths and sizes of vortex structures on loop E are stronger and larger. This is because loop E locates at the end of the strips and is close to the air conditioner, which will cause greater disturbance to the airflow. In addition, what can be observed from the figures is that, under the interference of the bogie, strong vortex structures are formed at the bottom of two loops, but their trajectories are obviously different. The vortex structures at the bottom of loop D mostly move along the direction of about 135° of the bogie until it merge with the airflow from the top. And the vortex structures at the bottom of the E loop will develop along the direction of about 225° of the bogie. Comparing Fig. 17a and b, it can be found that the strong vortex structures on the top of the smooth model initially moves close to the wall, while rectangular strips can make it move away from the wall for a certain distance and weaken the effect of turbulence in the boundary layer. Meanwhile, the blocking effect of the strips can reduce the instantaneous cross flow caused by the turbulent motion, and promote the splitting of the large vortex structures into smaller vortex structures, thereby significantly reducing the vorticity amplitude. From Fig. 17c and d, this conclusion can be seen more intuitively.

In summary, compared with the rough model, the strengths of vortex structures around the smooth model are stronger and the sizes of the vortex cores are larger, which is the key factor leading to the poor aerodynamic performance. The rectangular strips can ensure a more stable development of low-speed airflow by reducing the flow velocity and turbulence disturbance near the wall. This is the fundamental reason why the rough model has better crosswind stability.

Table 3 Results of C_s and C_{mz} for smooth and rough models

	C_s	C_{mz}
Smooth model	−2.075	−0.022
Rough model	−1.998	−0.020
RD	−3.7%	−9.1%

4.3 Characteristics of aerodynamic loads

After comparing the flow details between the smooth and rough models, it's worth making a comparison of the integration variables between both models. Experience has shown that side force and roll moment have a great influence on the safety of trains under cross wind. To simplify analysis, define side force coefficient C_s and roll moment coefficient C_{mz} as follows:

$$C_s = \frac{F_s}{0.5\rho V_{ref}^2 A_{ref}}, \tag{3}$$

$$C_{mz} = \frac{M_z}{0.5\rho V_{ref}^2 A_{ref} H_{ref}}, \tag{4}$$

where $A_{ref} = 0.1232\ m^2$ [9] is the projected area of the train in the x direction. H_{ref} is the train carriage height. F_s is the side force. M_z is the roll moment, and the moment center is at point (0, 0.07155, 0), as shown in Fig. 11.

Table 3 gives time-averaged results of C_s and C_{mz} for smooth and rough models. It can be seen that side force coefficient and roll moment coefficient of the rough surface model are smaller by 3.7% and 9.1% than the smooth model, indicating that the train with certain roughness can operate more safely and stably, which is consistent with the conclusion obtained from flow field analysis.

5 Conclusions

This paper aims to investigate the effects of roughness on the flow field details around the train surface and the aerodynamic characteristics of a train subjected to crosswinds. To do so, experimental and numerical work was conducted on a train body with a smooth surface and a rough surface at a yaw angle of 90°. The following conclusions can be drawn from the analysis:

(1) Despite the height of the added roughness with respect to the train height being less than 0.7%, it appears that the strips have an influence on the pressure distribution around the train, with mainly differences seen in the roof and leeward regions.

(2) For most of the loops, it is evident that the C_p values are lower for the rough roof surface as compared to the smooth roof surface, with the maximum RD being 59%.

(3) Increasing the strips can effectively restrain the separation phenomenon. The specific performance of the weakening of the flow separation is that the area where the flow separation occurs decreases and the surface pressure of the train decreases.

(4) The roughness can greatly dissipate the eddies around the LWS of the car, which achieves the purpose of improving the stability of train operation to a certain extent.

(5) Compared with the smooth model, the rough model can reduce the value of side force coefficient and roll moment coefficient by 3.7% and 9.1%.

The results of current research show that adding appropriate roughness to the train surface is a possible way to achieve aerodynamic optimization.

Acknowledgements The work was financed by the program of China Scholarships Council, Youth Innovation Promotion Association CAS (2019020), a University of Birmingham (UK) funded scholarship and was supported by the EU H2020 project LiftTRAIN (701693). The authors would also like to thank Professor Mohammad Mehdi Rashidi for his support in this project.

References

1. Ryder, A.: High speed rail. J. Transport Geogr. **22**, 303–305 (2012)
2. RSSB: Leading Health and Safety on Britain's Railway. Rail Safety and Standards Board Ltd, London (2016)
3. Diedrichs, B.: On computational fluid dynamics modelling of crosswind effects for high-speed rolling stock. Proc. Inst. Mech. Eng. F **217**(3), 203–226 (2003)
4. Hashmi, S.S.A., Hemida, S.D.: Wind tunnel testing on a train model subjected to crosswinds with different windbreak walls. J. Wild Eng. Ind. Aerodyn. **195**, 104013 (2019)
5. Browand, F., Ross, J., McCallen, R.: The Aerodynamics of Heavy Vehicles II: Trucks, Buses, and Trains. Springer, Berlin (2009)
6. EC. TSI—technical specification for Interoperability of the trans-European high-speed rail system, 'rolling stock' sub-system, TSI-HS2008/232/EC. Off. J. Eur. Union (2008)
7. RSSB: Resistance of Railway Vehicles to Roll-Over in Gales, Railway Group Standard GM/RT 2142. Rail Safety and Standards Board Ltd, London (2009)
8. CEN. Railway applications - Aerodynamics - Part 6: Requirements and test procedure for cross wind assessment. PrEN 14067-6 2009-02. CEN/TC 256 (2018)
9. Dorigatti, F., Sterling, M., Baker, C., et al.: Crosswind effects on the stability of a model passenger train—a comparison of static and moving experiments. J. Wind Eng. Ind. Aerodyn. **138**, 36–51 (2015)
10. Chen, Z.W., Liu, T.H., Li, W.H.: Numerical analysis of different nose shapes on the train aerodynamic performance at a windbreak transition under crosswinds. J. Appl. Math. Phys. **08**(11), 2519–2525 (2020)

11. Miao, X.J., He, K., Minelli, G., et al.: Krajnovic. Aerodynamic performance of a high-speed train passing through three standard tunnel junctions under crosswinds. Appl. Sci. **10**(11), 3664 (2020)
12. Hemida, H., Krajnović, S.: LES study of the influence of the nose shape and yaw angles on flow structures around trains. J. Wind Eng. Ind. Aerodyn. **98**(1), 34–46 (2009)
13. Cheli, F., Corradi, R., Rocchi, D., et al.: Wind tunnel tests on train scale models to investigate the effect of infrastructure scenario. J. Wind Eng. Ind. Aerodyn. **98**(6), 353–362 (2010)
14. Wang, J.G., Chen, S.H., Wang, Q.J.: Effect of bionic rhombic surface texture on frictional noise of high-speed train. J. Traffic Transport. Eng. **14**(01), 43–48 (2014). (In Chinese)
15. Miao, X.J., Gao, G.J.: Influence of ribs on train aerodynamic performances. J. Cent. S. Univ. **22**(5), 1986–1993 (2015)
16. Zhang, Y., Zhang, J.Y., Li, T.: Research on the drag reduction characteristics of high-speed train with non-smooth surface. Des. Res. **43**(09), 12–15 (2016). (In Chinese)
17. Zhu, H.Y., Zhang, Y., Zhao, H.R., et al.: Drag reduction technology of high-speed train based on boundary layer control. J. Traffic Transport. Eng. **17**(02), 64–72 (2017). (In Chinese)
18. García, J., Muñoz-Paniagua, J., Crespo, A.: Numerical study of the aerodynamics of a full scale train under turbulent wind conditions, including surface roughness effects. J. Fluids Struct. **74**, 1–8 (2017)
19. Liu, H.T., Xu, Z.L.: Study on drag and noise reduction of pantograph rods based on bionic non-smooth structures. Noise Vibrat. Control **38**(z1), 269–272 (2018). (In Chinese)
20. Tang, K., Ma, S.W., Liang, H.Q., et al.: Simulation research of the drag reduction of high-speed train microstructured surfaces. Mach. Des. Manufact. **09**, 213–216 (2020). (In Chinese)
21. TFI.: Turbulent Flow Instrumentation-Cobra Probe - Getting started guide. Technical report (2011)
22. Hemida, H., Krajnović, S., Davidson, L.: Large-Eddy simulation of the flow around a simplified high speed train under the influence of a cross-wind. AIAA J. (2005). https://doi.org/10.2514/6.2005-5354
23. Biadgo, A.M., Simonovic, A., Svorcan, J., et al.: Aerodynamic characteristics of high speed train under turbulent cross winds: a numerical investigation using unsteady-RANS method. Facul. Mech. Eng. **42**, 10–18 (2014)
24. Spalart, P.R., Garbaruk, A., Strelets, M.: RANS solutions in Couette flow with streamwise vortices. Int. J. Heat Fluid Flow **49**, 128–134 (2014)
25. Gritskevich, M.S., Garbaruk, A.V., Schütze, J., et al.: Development of DDES and IDDES formulations for the k-ω Shear Stress Transport Model. Flow Turbul. Combust **88**, 431–449 (2012)
26. Li, T.: Comparisons of shear stress transport and detached eddy simulations of the flow around trains. J. Fluids Eng. **14**, 11 (2018)

Publisher's Note Springer Nature remains neutral with regard to jurisdictional claims in published maps and institutional affiliations.